Submitted to

31st International Conference on High Energy Physics, ICHEP02, July 24, 2002, Amsterdam

Abstract: **984**

Parallel Session **6**

www-h1.desy.de/h1/www/publications/conf/conf_list.html

Measurement of Semi-Inclusive Diffractive Deep-Inelastic Scattering with a Leading Proton at HERA

H1 Collaboration

Abstract

The semi-inclusive cross section for the diffractive deep-inelastic scattering process $ep \to eXp'$ is studied with a leading proton detected in the H1 forward proton spectrometer. The results are presented in terms of the differential cross section $\mathrm{d}\sigma/\mathrm{d}t$ and the diffractive structure function $F_2^{D(3)}(x_{I\!P}, \beta, Q^2)$ measured in the kinematic range $2 < Q^2 < 50$ GeV^2, $5 \cdot 10^{-3} < \beta < 1$, $x_{I\!P} < 0.09$ and $-0.45 < t < -0.08$ GeV^2.

1 Introduction

The observation of events with a large rapidity gap in the distribution of the final state hadrons at HERA [1] allows the nature of colour singlet exchange in strong interactions to be investigated. Colour singlet exchange interactions have been successfully modelled in terms of phenomenological Regge theory [2] and, at high energy, are attributed to diffractive or pomeron exchange. HERA allows the partonic nature of diffraction to be investigated in deep–inelastic scattering (DIS) using the virtual photon as a probe.

In diffractive DIS events at HERA [3, 4], where $ep \rightarrow eXY$, the photon dissociation system X and the proton remnant system Y are separated by a large gap in rapidity. The system X (with mass M_X) is usually reconstructed in the central detector and, by requiring the absence of particles in the forward region of the detector, the mass of the proton remnant system M_Y and the square of the four-momentum transfer at the proton vertex t are restricted to small values ($|t| < 1$ GeV^2, $M_Y < 1.6$ GeV). Diffractive DIS single dissociation events ($ep \rightarrow eXp'$) are also measured at HERA [5, 6] by directly observing the final state proton using proton spectrometers located close to the beam-line. The detection of the final state proton facilitates the measurement of the differential cross section $\mathrm{d}\sigma/\mathrm{d}t$ and reduces the large uncertainty in the contribution of proton disociative processes present in the large rapidity gap method.

The semi-inclusive structure function $F_2^{LP(3)}(x_{I\!P}, x, Q^2)$ [6] was measured with a leading proton detected by the H1 forward proton spectrometer (FPS) in the range $x_{I\!P} > 0.1$. In this paper a new measurement of the diffractive structure function $F_2^{LP(3)}$ is presented which extends the kinematic range to values of $x_{I\!P} < 0.1$. At these low values of $x_{I\!P}$ the measurement can be directly compared with measurements of $F_2^{D(3)}(x_{I\!P}, \beta, Q^2)$ [7] obtained using the presence of a rapidity gap in the central detector. The differential cross section $\mathrm{d}\sigma/\mathrm{d}t$ is also measured for four different $x_{I\!P}$ values.

The present analysis is based on H1 data collected in the running period from January to April 1999, when HERA collided 920 GeV protons with 27.5 GeV electrons, and in the running period from August 1999 to August 2000, when 27.5 GeV positrons were collided instead of electrons.

2 The Forward Proton Spectrometer

The FPS [8] is used to measure the four momentum of the scattered proton. Protons scattered at small angles to the incident proton direction are deflected by the magnets of the beam optics into a system of detectors placed close to the proton beam. The detectors consist of fibre hodoscopes, sandwiched between trigger scintillators, installed in movable "Roman Pot" plunger vessels. Two identical stations are installed at 64 m and 80 m away from the interaction point[1]. The absolute energy scale uncertainty is estimated as ± 5.5 GeV, which is about 0.6% of the proton beam energy. The distance of the detectors from the beam and the beam line aperture restrict the FPS acceptance in the squared 4-momentum transferred between the incident proton and the final state leading proton to $-0.45 < t < -0.08$ GeV^2 and $E_{p'}/E_p > 0.9$, where $E_{p'}$ is the energy of the leading proton and E_p is the proton beam energy.

[1]At 81 m and 90 m two more detectors are installed. Due to a different acceptance these are not used in the present analysis.

3 Event Selection

The data analysed in this paper were restricted to running periods where the FPS detectors were in a stable position close to the circulating beam and all relevant components of the H1 detector were fully operational. The corresponding luminosity amounts to $28.8\ \mathrm{pb}^{-1}$. The event selection is based on the reconstruction of a proton track in the FPS, an electron candidate with energy above $10\ \mathrm{GeV}$ in the backward electromagnetic calorimeter (SPACAL) [9] and at least one reconstructed track in the central H1 detector [10]. At the trigger level, a signal in each of the components was required. In order to reject background from interactions of the beam with the residual gas in the beampipe, the z coordinate of the event vertex was restricted to $|z_{vtx}| < 35\ \mathrm{cm}$. In addition the quantities $\sum_i (E - P_z)$ and $\sum_i (E + P_z)$ which are calculated using the energy E_i and the longitudinal momentum $p_{z,i}$ of all final state particles including the scattered positron and proton were required to be greater than $35\ \mathrm{GeV}$ and less than $1880\ \mathrm{GeV}$ respectively. The contribution from photoproduction events has been estimated using the PHOJET Monte Carlo [11] and found to be negligible.

The phase space of the analysis is restricted to the range $2 < Q^2 < 50\,\mathrm{GeV}^2$, $0.01 < y < 0.6$ and $x_{I\!P} < 0.09$. The standard DIS variables Q^2, y and x are reconstructed using the double angle method. The variable $x_{I\!P}$ may be reconstructed using either the scattered proton measured in the FPS using $x_{I\!P} \simeq 1 - E_{p'}/E_p$ or the combination of the hadronic final state and scattered electron measured in the central detector $x_{I\!P} \simeq (Q^2 + M_X^2)/(Q^2 + W^2)$. In order to obtain the best resolution possible the FPS is used to reconstruct $x_{I\!P}$ for values $E_{p'}/E_p < 0.99$ and the central detector is used for values $E_{p'}/E_p > 0.99$. The squared four-momentum transferred at the proton vertex t is reconstructed from $t = -p_t^2/(1 - x_{I\!P}) - t_{min}$ using $x_{I\!P}$ and p_t^2 measured in the FPS. The final data sample, after all cuts, contains about 3100 events.

Monte Carlo simulations are used to correct the data for the effects of losses and migrations due to the finite resolution of the H1 detector. The smeared acceptance is calculated by running the H1 detector simulation program on a sample of events generated using an implementation of the 'Saturation' model [12] within the RAPGAP generator [13]. The cross section is corrected to the Born level and the radiative corrections are calculated using RAPGAP interfaced to HERACLES [14].

4 Systematic Uncertainties

Systematic uncertainties from the following sources are considered:

- The uncertainty in the FPS track reconstruction efficiency results in an overall normalisation uncertainty of 10% for the e^-p data, 12% for e^+p data collected in 1999 and 20% for e^+p data collected in 2000.
- The uncertainties in the reconstruction of the energy and transverse momentum of leading proton is estimated by shifting $E_{p'}$ by ± 2 GeV and p_t by $\pm 10\ \mathrm{MeV}$.

- The uncertainty in the reconstruction of the scattered electron is estimated by changing the electromagnetic energy scale of the SPACAL by $\pm 2\%$ and shifting the electron polar angle by ± 2 mrad.
- The uncertainty in the reconstruction of the hadronic final state is estimated by changing the hadronic energy scale of the LAr calorimeter by $\pm 4\%$ and the energy fraction carried by the tracks by $\pm 3\%$.
- The uncertainty in the physics model used to compute the acceptance corrections is estimated by reweighting the generated $x_{I\!P}$ distribution by $x_{I\!P}^{\pm 0.2}$, the β distribution by $(1 \pm 0.3\beta)$ and the t distribution by $e^{\pm 2t}$.
- The uncertainty in the trigger efficiency is estimated by comparing the trigger efficiency obtained from a sample of independently triggered data events with that in the simulation.

5 The Differential Cross Section $\mathrm{d}\sigma/\mathrm{d}t$

The differential cross section $\mathrm{d}\sigma/\mathrm{d}t$ is measured for 4 ranges of $x_{I\!P}$ and shown in figure 1. For each $x_{I\!P}$ range the dependence of the cross section on t is parameterised as $\mathrm{d}\sigma/\mathrm{d}t \propto e^{Bt}$ and is shown as a solid line on the figures. The extracted slope parameter B is plotted as a function of $x_{I\!P}$ in figure 2. Within the experimental errors no dependence on $x_{I\!P}$ is visible. The mean value of the slope parameter B in the kinematic range $2 < Q^2 < 50\ \mathrm{GeV}^2$, $0.01 < y < 0.6$, $-0.45 < t < -0.08$ GeV and $x_{I\!P} < 0.09$ is $B = 5.0 \pm 0.3(\mathrm{stat.}) \pm 0.8\ (\mathrm{syst.})\ \mathrm{GeV}^{-2}$. The results are consistent within errors with measurements made using the ZEUS LPS [5], made in a similar kinematic range, which are also shown in figure 2.

6 Measurement of $F_2^{LP(3)}$ and $F_2^{D(3)}$

In order to compare with the result of the previous H1 FPS measurement of the structure function $F_2^{LP(3)}(x_{I\!P}, x, Q^2)$ performed at high $x_{I\!P}$ [6], the data are extrapolated into the range $p_t < 0.2$ GeV using the t dependence measured in section 5. The results are shown in figure 3. The combined data points cover the $x_{I\!P}$ range $2 \cdot 10^{-3}$ to 0.27 and show the transition from diffractive DIS processes with $\mathbb{P}$ exchange ('flat' behaviour of $F_2^{D(3)}$ at $x_{I\!P} < 0.05$) to processes which involve dominantly $\mathbb{R}$ and π exchange (rising $F_2^{LP(3)}$ behaviour at $x_{I\!P} > 0.05$). The prediction of the 'Saturation' model [12], as implemented in the RAPGAP Monte Carlo generator, is compared with the new measurement and is found to be in good agreement with the data.

The H1 FPS data may also be plotted as a function of $x_{I\!P}$ at fixed values of β and Q^2 to give the diffractive structure function $F_2^{D(3)}(x_{I\!P}, \beta, Q^2)$. The structure function $F_2^{D(3)}$ is presented in figure 4 integrated over the t range $-0.45 < t < -0.08\ \mathrm{GeV}^2$.

The diffractive structure function $F_2^{D(3)}(x_{I\!P}, \beta, Q^2)$ has also been reecently measured [7], using the presence of a large rapidity gap in the central detector, and corrected to the range

$M_Y < 1.6$ GeV and $|t| < 1$ GeV^2. In order to compare with this data the FPS measurement of $F_2^{D(3)}(x_{I\!P}, \beta, Q^2)$ is extrapolated into the range $|t| < 1$ GeV using the t slope measured in section 5. The extrapolation in t is about a factor of 2 with an uncertainty of 15% which comes from the error on the measurement of the slope parameter B. Studies using simulations of the DIFFVM [15] generator show that the fraction of leading protons from proton dissociation is around 5% in the highest measured $x_{I\!P}$ bin ($0.05 < x_{I\!P} < 0.09$) and negligible for lower $x_{I\!P}$ values. The comparison of the structure function obtained from the 2 different methods is shown in figure 5. Within errors the leading proton data are in good agreement with the data obtained independently from the requirement of a rapidity gap in the central detector, indicating that the contribution of proton dissociation in the range $M_Y < 1.6$ GeV is small. In addition, the FPS data extend the kinematic range of $F_2^{D(3)}$ into the low β ($\beta = 0.01$) and low Q^2 ($Q^2 = 2.6$ GeV^2) regions.

In figure 6 the diffractive structure function $F_2^{D(3)}(x_{I\!P}, \beta, Q^2)$ with a leading proton detected in the FPS is compared with the predictions of two versions of the 'Saturation' model [12, 16]. Within the experimental errors both versions of the model are able to give a reasonable description of the data over the whole Q^2 and β range of the measurement.

7 Conclusions

The differential cross section $\mathrm{d}\sigma/\mathrm{d}t$ and the structure functions $F_2^{LP(3)}(x_{I\!P}, x, Q^2)$ and $F_2^{D(3)}(x_{I\!P}, \beta, Q^2)$ have been measured in diffractive DIS processes with a leading proton detected in the H1 forward proton spectrometer. A fit to the differential cross section $\mathrm{d}\sigma/\mathrm{d}t \propto e^{Bt}$ yields a slope parameter $B = 5.0 \pm 0.3$ (stat.) $\pm\ 0.8$ (syst.) GeV^{-2} in the range $2 < Q^2 < 50$ GeV^2 , $0.01 < y < 0.6$, $-0.45 < t < -0.08$ GeV and $x_{I\!P} < 0.09$.

Comparison of the data with $F_2^{LP(3)}(x_{I\!P}, x, Q^2)$ previously measured by H1 FPS in the high $x_{I\!P}$ or non-diffractive range show behaviour consistent with the transition from $\mathbb{P}$ exchange at $x_{I\!P} < 0.05$ to the dominance of $\mathbb{R}$ and π exchange at $x_{I\!P} > 0.05$.

Comparison of the leading proton data with $F_2^{D(3)}(x_{I\!P}, \beta, Q^2)$ obtained from the presence of a large rapidity gap in the central detector shows good agreement between the two methods. The 'Saturation' model is able to give a good description of the new leading proton data.

References

[1] M. Derrick *et al.* [ZEUS Collaboration], Phys. Lett. B **315** (1993) 481.
T. Ahmed *et al.* [H1 Collaboration], Nucl. Phys. B **429** (1994) 477.

[2] T. Regge, Nuovo Cim. **14** (1959) 951.

[3] H1 Collaboration, C.Adloff *et al.* Z. Phys. **C 76** (1997) 613.

[4] J. Breitweg *et al.* [ZEUS Collaboration], Eur. Phys. J. C **6** (1999) 43 [hep-ex/9807010].

[5] ZEUS Collaboration, J. Breitweg *et al.*, Eur. Phys. J. **C 1** (1998) 81.
ZEUS Collaboration, *Diffractive Results from the ZEUS Leading Proton Spectrometer at HERA*, Talk given by B. Smalska at the 9^{th} *International Workshop on Deep Inelastic Scattering*, Bologna, Italy, April 27-May 1, 2001.

[6] H1 Collaboration, C.Adloff *et al.* Eur. Phys. J. **C 6** (1999) 587.

[7] H1 Collaboration, *Measurement of the diffractive structure function* $F_2^D(3)$, Abstract 808, Paper submitted to *International Europhysics Conference on High Energy Physics*, Budapest, Hungary, July 12-18, 2001.

[8] P. Van Esch *et al.*, Nucl. Instrum. Meth. A **446** (2000) 409.

[9] R. D. Appuhn *et al.* [H1 SPACAL Group Collaboration], Nucl. Instrum. Meth. A **386** (1997) 397.

[10] I. Abt *et al.* [H1 Collaboration], Nucl. Instrum. Meth. A **386** (1997) 310.

[11] R.Engel, Z. Phys. **C 66** (1995) 203.

[12] K. Golec-Biernat, M. Wüsthoff, *Phys. Rev.* **D 59** (1999) 014017;
K. Golec-Biernat, M. Wüsthoff, *Phys. Rev.* **D 60** (1999) 114023.

[13] H.Jung, Comp.Phys.Commun. **86** (1995) 147.

[14] A.Kwiatkowski *et al.*, Comp.Phys.Commun. **69** (1992) 155.

[15] B.List, Diploma Thesis (Tech. Univ. Berlin, 1993 (unpublished).

[16] K. Golec-Biernat, M. Wüsthoff, *Eur. Phys. J.* **C 20** (2001) 313.

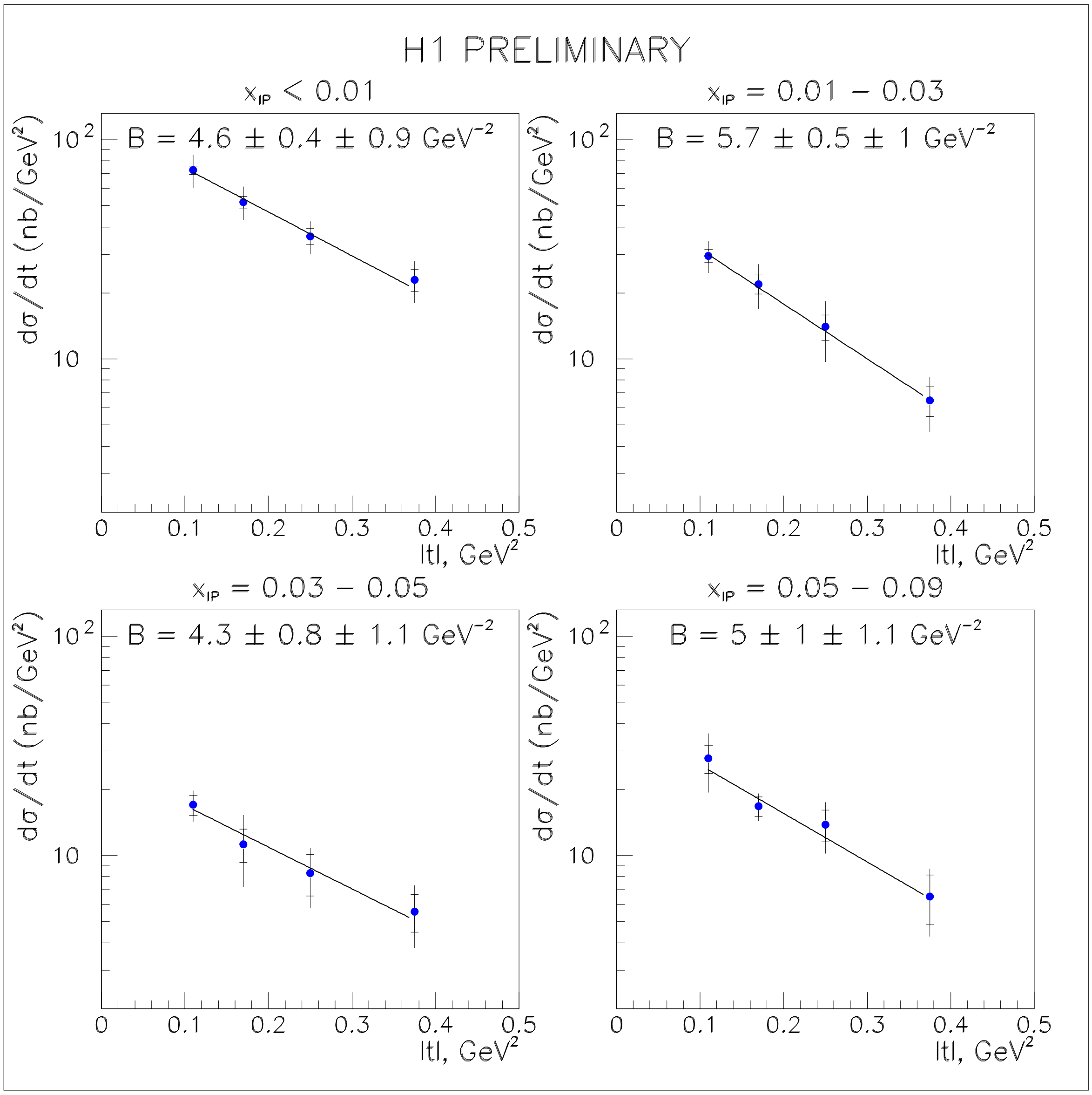

Figure 1: The differential cross section $\mathrm{d}\sigma/\mathrm{d}t$ measured with the H1 FPS in the range $2 < Q^2 < 50\ \mathrm{GeV}^2$, $0.01 < y < 0.6$, $5 \cdot 10^{-3} < \beta < 1$ for four different $x_{I\!P}$ bins. Results of the fit with a function $\mathrm{d}\sigma/\mathrm{d}t \propto e^{Bt}$ are shown. The inner error bars represent the statistical errors, the outer error bars the statistical and systematic errors added in quadrature.

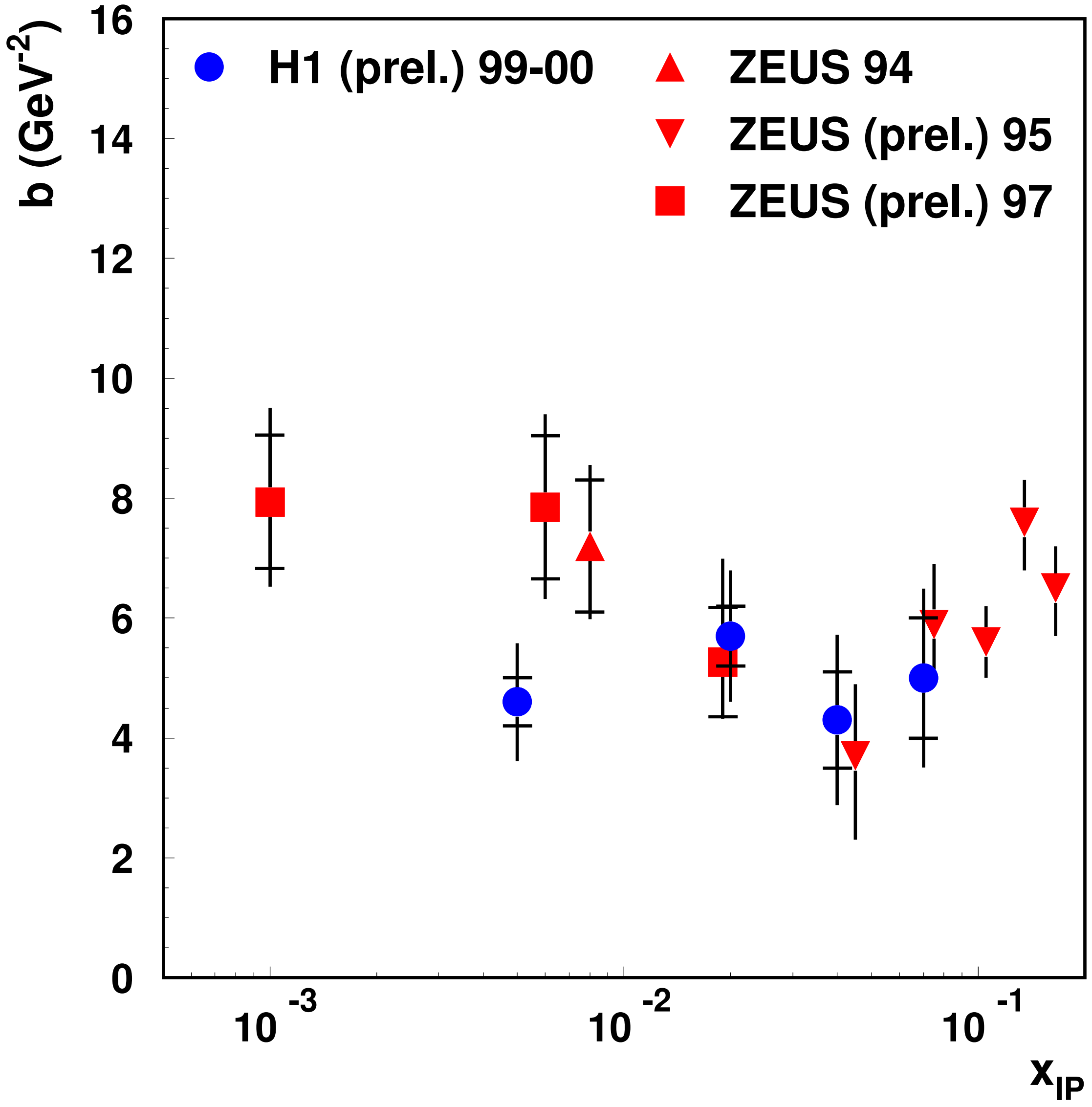

Figure 2: The slope parameter B of the differential cross section $\mathrm{d}\sigma/\mathrm{d}t \propto e^{Bt}$ as a function of $x_{I\!P}$. Results using the ZEUS LPS [5] are also shown. The inner error bars represent the statistical errors; the outer error bars the statistical and systematic errors added in quadrature.

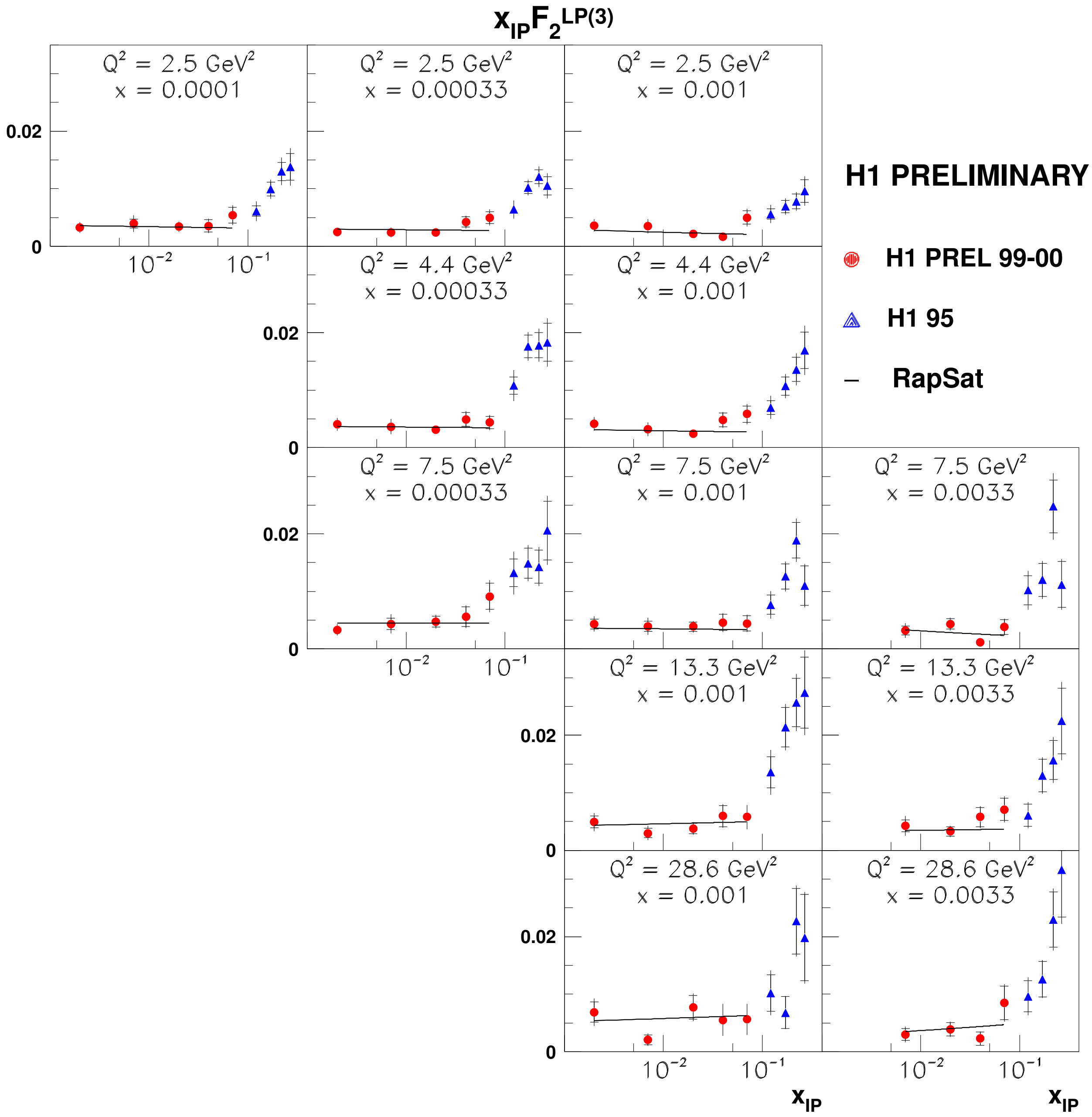

Figure 3: The structure function $F_2^{LP(3)}(x_{I\!P}, x, Q^2)$, presented as $x_{I\!P}F_2^{D(3)}(x_{I\!P}, x, Q^2)$ and plotted as a function of $x_{I\!P}$ at fixed values of x and Q^2. The circles are new data measured with a leading proton detected in the FPS extrapolated into the range $p_t < 0.2$ GeV. The results of the previous H1 leading proton measurement [6] performed at larger values of $x_{I\!P}$, in the same p_t range, are shown as triangles. The solid curve shows the prediction of the 'Saturation' model as implemented in the RAPGAP Monte Carlo generator. The inner error bars represent the statistical errors; the outer error bars the statistical and systematic errors added in quadrature.

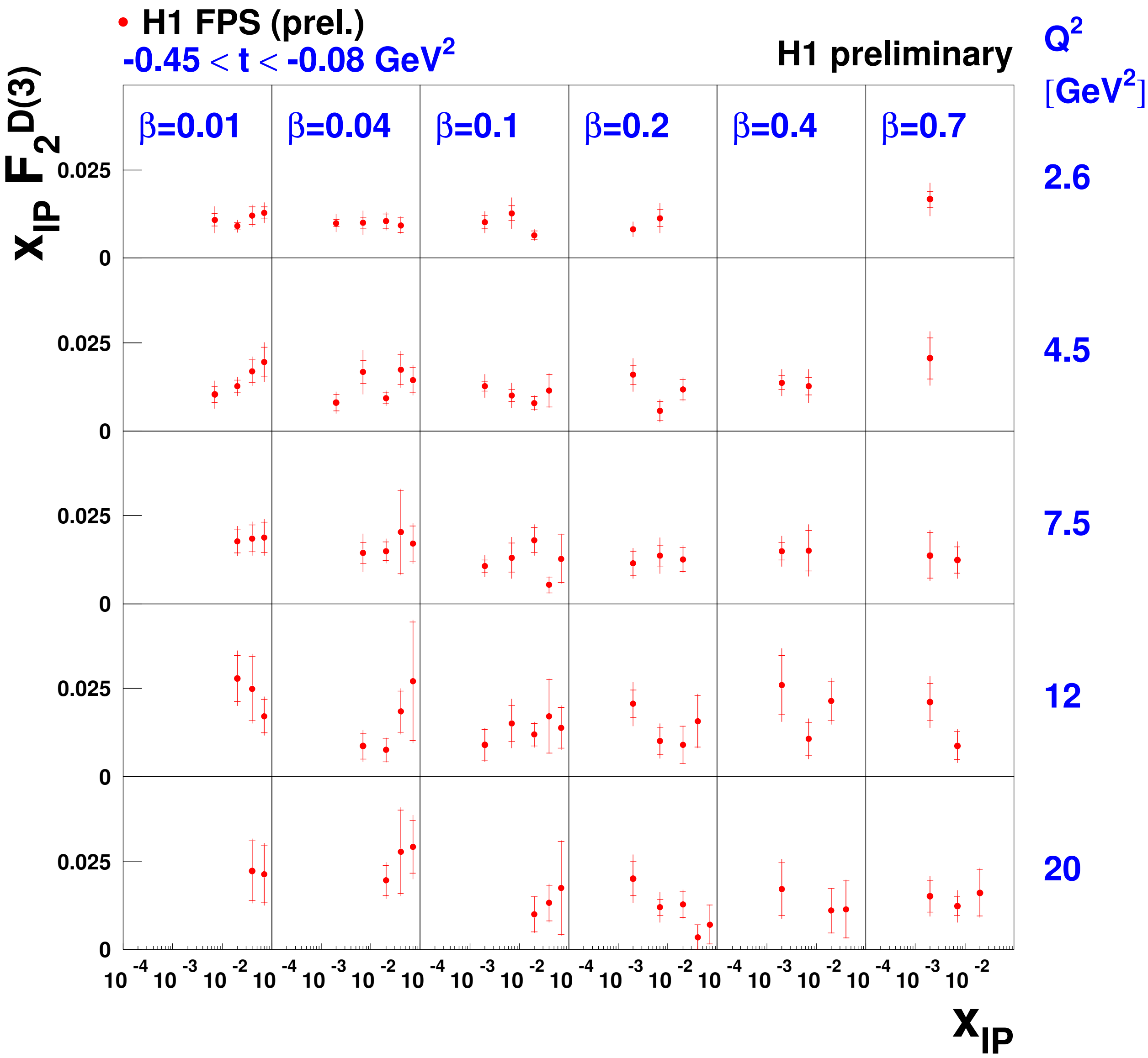

Figure 4: The structure function $F_2^{D(3)}(x_{I\!P}, \beta, Q^2)$ presented as $x_{I\!P} F_2^{D(3)}(x_{I\!P}, \beta, Q^2)$ and plotted as a function of $x_{I\!P}$ at fixed values of β and Q^2. The squares are data with a leading proton detected in the FPS, in the range $-0.45 < t < -0.08$ GeV^2. The inner error bars represent the statistical errors; the outer error bars the statistical and systematic errors added in quadrature.

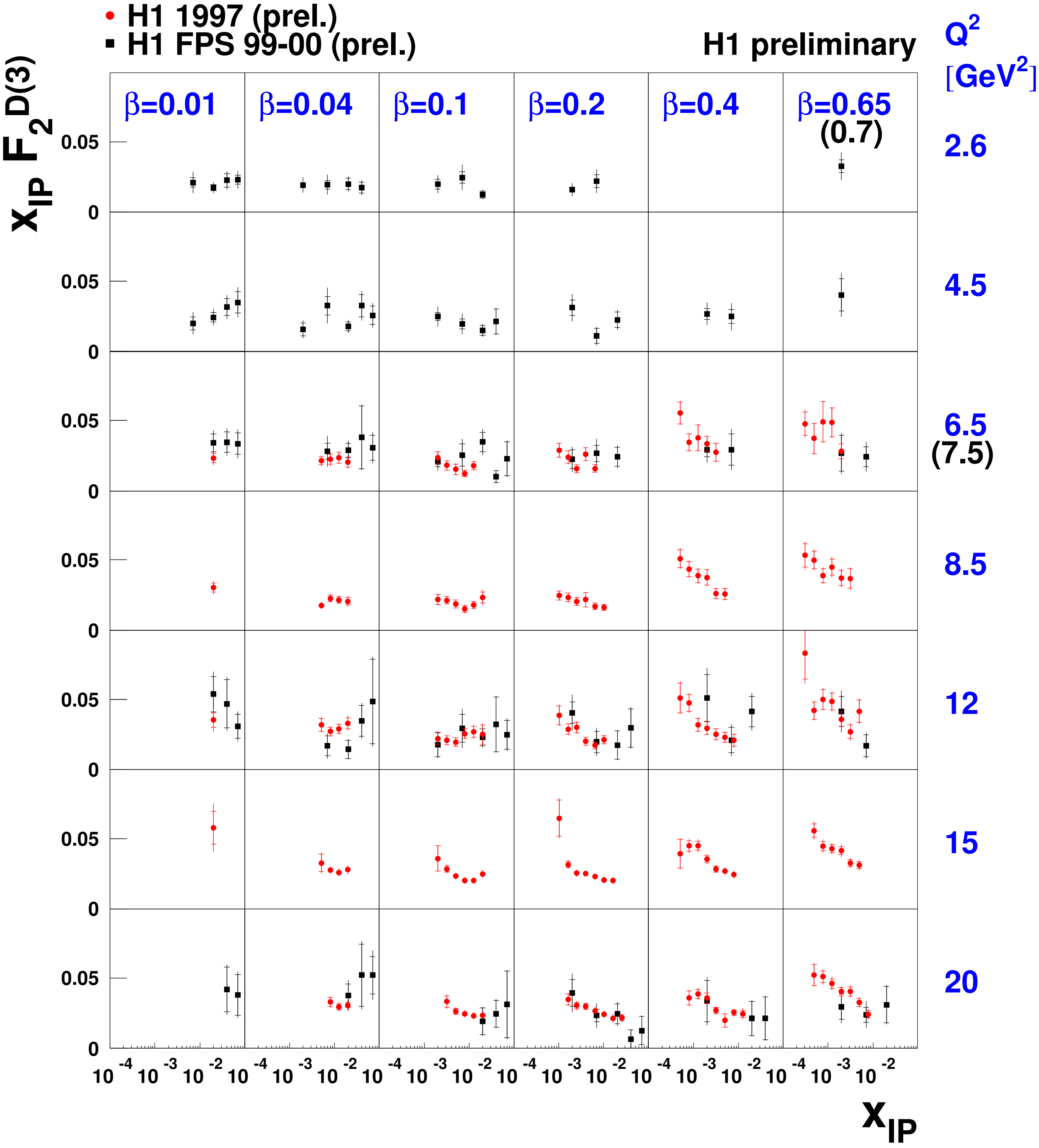

Figure 5: The structure function $F_2^{D(3)}(x_{I\!P}, \beta, Q^2)$ presented as $x_{I\!P} F_2^{D(3)}(x_{I\!P}, \beta, Q^2)$ and plotted as a function of $x_{I\!P}$ at fixed values of β and Q^2. The squares are data with a leading proton detected in the FPS, extrapolated into the range $|t| < 1$ GeV^2. The results of the preliminary H1 measurement of $x_{I\!P} F_2^{D(3)}$ in processes with a large rapidity gap are shown as circles. The leading proton data at $Q^2 = 20$ GeV^2 and $\beta = 0.7$ are compared with rapidity gap data at $Q^2 = 18$ GeV^2 and $\beta = 0.65$ respectively. The inner error bars represent the statistical errors; the outer error bars the statistical and systematic errors added in quadrature.

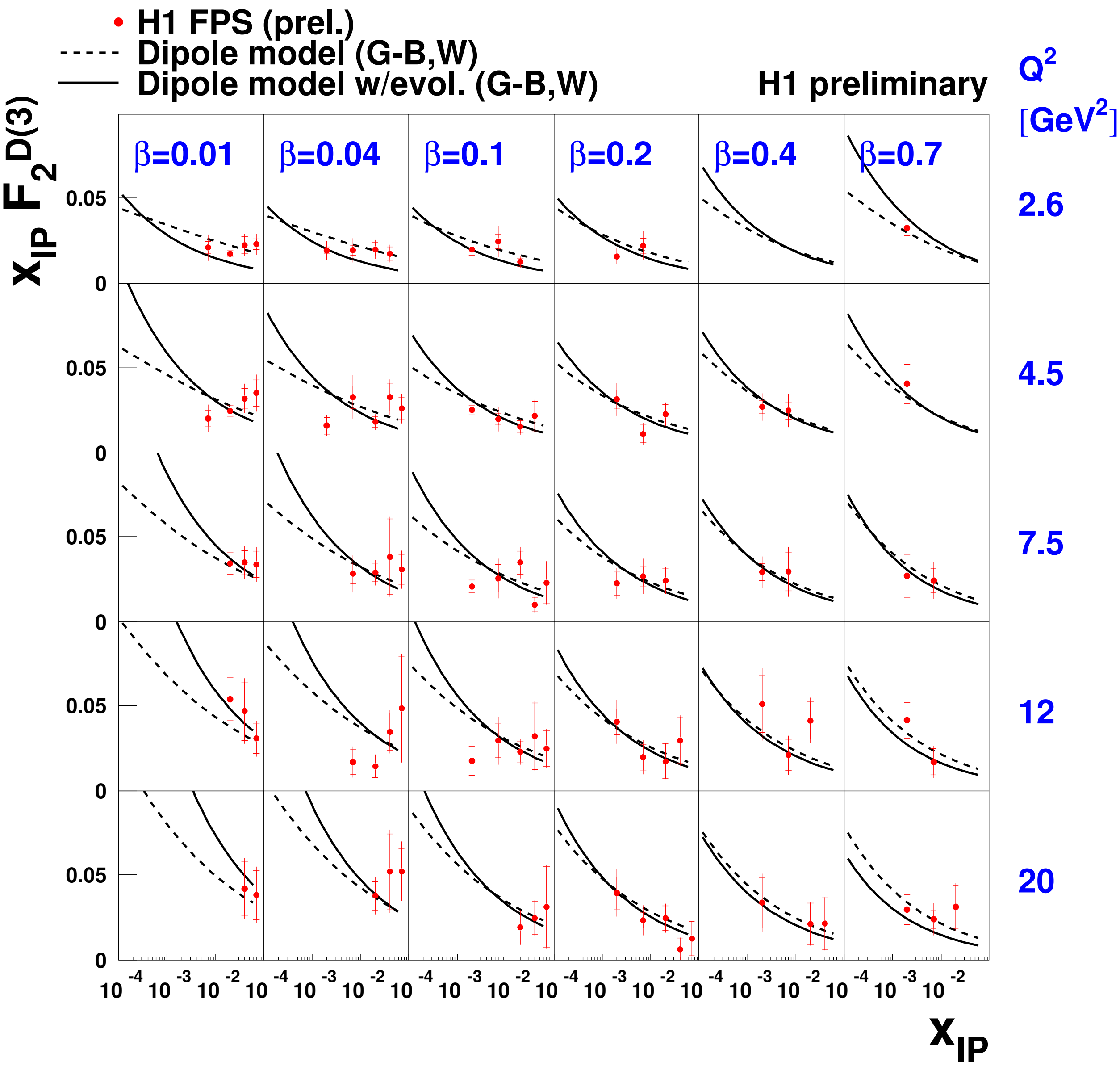

Figure 6: The structure function $F_2^{D(3)}(x_{I\!P}, \beta, Q^2)$ presented as $x_{I\!P} F_2^{D(3)}(x_{I\!P}, \beta, Q^2)$ and plotted as a function of $x_{I\!P}$ at fixed values of β and Q^2. The squares are data with a leading proton detected in the FPS, extrapolated into the range $|t| < 1$ GeV^2. The data are compared with two versions of the 'Saturation' model [12, 16]. The inner error bars represent the statistical errors; the outer error bars the statistical and systematic errors added in quadrature.